Crystallization kinetics and morphological features of star-branched nylon-6: effect of branch-point functionality

Brian G. Risch and Garth L. Wilkes*
Department of Chemical Engineering, Polymer Materials and Interfaces Laboratory, Virginia Polytechnic Institute and State University, Blacksburg, VA 24061, USA

and John M. Warakomski
Designed Thermoplastics Research Laboratory, The Dow Chemical Company, Midland, MI 48667, USA
(Received 24 March 1992; revised 4 September 1992)

Bulk crystallization rates, nucleation density, general morphological features, equilibrium melting point and absolute crystalline percentage of linear and star-branched nylon-6 have been studied as a function of branch-point functionality and temperature. Overall bulk crystallization rates were described in terms of the Avrami equation and crystallization half-times. No significant differences in bulk crystallization rates as a function of crystallization temperature or absolute crystalline percentage were observed between linear, three-arm and six-arm samples with identical thermal history. Equilibrium melting points obtained by Hoffman Weeks analysis were reduced in star-branched nylon-6 compared to the linear polymer of comparable molecular weight. In order to deconvolute the effects of a decreased thermodynamic driving force for formation of crystals of branched polymers, crystallization half-times were measured as a function of supercooling. The crystallization half-times of star-branched nylon-6 as a function of *supercooling* were reduced compared to those of linear nylon-6 of comparable molecular weight. The general spherulitic superstructure appeared unaffected by increasing branch-point functionality up to six. However, irregularities in lamellar structure were implied by SAXS experiments on samples with branch-point functionality as low as three.

(Keywords: crystallization; kinetics; morphology)

INTRODUCTION

Linear nylon-6 has been a widely available, commercially important polymer for years. Star-branched nylon-6 varies from the linear variety in that it is characterized by a branch point from which a number of polymer chains or arms emanate. Recently, there has been increasing interest in starburst 'dendrimers', a new class of molecules possessing extraordinary symmetry as well as high branching and terminal functionality[1-4]. Star-branched nylon-6 with precisely controlled branching has been synthesized using starburst dendrimers as branch points[5]. This new class of star-branched polymers offers significant reduction in melt viscosity compared to linear nylon-6 of comparable molecular weight. This reduction of melt viscosity allows for processing at lower temperatures and pressures as well as the ability to process higher molecular weight polymers. Additionally, reduced viscosity allows for improved extrudability as well as injection moulding of nylon-6.

The solid state properties of both linear and star branched nylon-6 depend on the crystallization behaviour and morphology of the polymer. Extensive studies have been performed on the thermodynamic and structural properties of linear nylon-6[6-13]. However, the effects of 'dendrimer' star-branching on the crystallization kinetics and morphology of nylon-6 has, until now, remained uninvestigated. Mathias and Sikes[14,15] have investigated the chemical structure and some of the physical properties of star-branched nylon-6 synthesized by an alternative means. They synthesized a star-branched polymer with branch point functionality of three, but had difficulty in controlling molecular weight and preventing crosslinking reactions from occurring. An earlier study on the crystallization kinetics of hydrogenated polybutadiene (HPB) had found that star-branching in HPB with $(M_w/M_e) \approx 10$, where M_e is the average molecular weight between molecular entanglements, had the same effect as reducing the molecular weight by one-third[16]. Both these studies, however, lacked the precise control of branch-point functionality possible with starburst dendrimers. They also did not investigate the effects of increasing branch-point functionality on morphological features, as well as on equilibrium melting point and absolute crystallinity. The objective of this research has been to determine the effects, if any, that star-branching has on crystallization kinetics and morphology as

* To whom correspondence should be addressed

0032-3861/93/112330-14

well as thermodynamic properties such as equilibrium melting point. While keeping the number average degree of polymerization constant, the effect of changing branch-point functionality from 2 (i.e. linear) to 3–6 was investigated by means of optical polarized microscopy (OPM), scanning electron microscopy (SEM), small angle light scattering (SALS), wide angle X-ray diffraction (WAXD), small angle X-ray scattering (SAXS) and transmission electron microscopy (TEM), as well as differential scanning calorimetry (d.s.c.).

EXPERIMENTAL

The samples utilized for the present study were prepared by a cation-initiated ring opening polymerization of ε-caprolactam with amine initiator functionality of two, three and six[5,17]. The initiators for the three- and six-arm systems were the above-mentioned starburst dendrimers first synthesized by Tomalia *et al.*[1]. The second-generation starburst polyethyleneimine used as an initiator for six-arm star-branched nylon-6 is shown in *Figure 1*. In the case of the linear polymer, 1,5-diamino pentane hydrochloride was used as an initiator. In all cases the chemical structure of the initiator is substantially different than that of the nylon-6 repeat unit. The unique nature of the branch-point structure differentiates this type of regular-star-branching from conventional long-chain branching where the chemical structure of the branch point is similar to that of the polymeric repeat unit.

Characterization information is outlined in *Table 1*. The number average degree of polymerization, *DP*, was estimated from the product of the fractional conversion and monomer to initiator ratio. G.p.c. experiments were performed on materials with similar nominal degrees of polymerization by Russo using linear nylon-6 as a calibration standard[18]. All nylon-6 samples were functionalized using a trifluoroacetylation reaction, in order to facilitate solvation in methylene dichloride[19,20]. M_n and M_w were estimated for the materials in this study by using the results obtained by Russo, which were corrected for the reduced hydrodynamic volume of the star-branched polymers. Correction for hydrodynamic volume was necessary because the mean square radius of gyration for star-branched *versus* linear polymers is known to scale as: $\langle R_g^2\rangle_{branched}/\langle R_g^2\rangle_{linear}=(3f-2)/f^2$, where f is the branch-point functionality[21]. Polyamides functionalized using the trifluoroacetylation procedure are

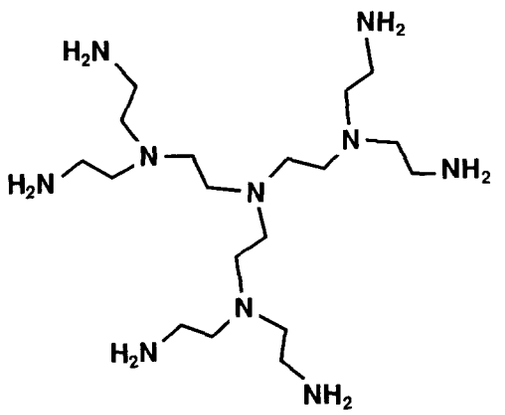

Figure 1 Chemical structure of the second-generation starburst polyethyleneimine used as an initiator in six-arm nylon-6

Table 1 Characteristics of samples utilized to study the effect of branch-point functionality on the crystallization kinetics and morphology of nylon-6

Sample designation	Initiator functionality	Number average DP^a	$M_n{}^b$	$M_w{}^b$
Linear	2	270	16000	29000
Three-arm	3	300	19000	36000
Six-arm	6	270	21000	42000
Six-arm	6	1150	49000	105000

[a] Estimated from monomer to initiator ratio and fractional conversion
[b] Measured by g.p.c. analysis

easily hydrolysed shifting the molecular weight distribution to lower values as well as increasing dispersity[20]. On the other hand, the estimation of number average *DP* based on fractional conversion assumes that the polymerization reaction was a living polymerization. It is likely that the actual values of M_n for the samples lie somewhere between the values determined by g.p.c. and those determined by fractional conversion. For convenience, the samples will be referred to according to the number average degree of polymerization determined by fractional conversion.

Morphological studies

Reimschuessel *et al.*[7–10] have shown that polymers with strong secondary interactions such as hydrogen bonding in nylon-6 retain orientation memory at temperatures even above their equilibrium melting point. In order to minimize the effects of previous thermal and mechanical history, all samples were heated to 240°C, approximately 10°C above the equilibrium melting point, for 10 min prior to all morphological experiments. Samples were moulded into thin films between glass microscope cover slides in order to determine any differences in morphological features as a function of branching functionality by means of OPM and SALS. A Zeiss polarizing microscope equipped with a Leitz 350 heating stage and a 35 mm camera was utilized for OPM. SALS experiments were performed in a lightproof room, with a HeNe laser (6328 Å). An open-back camera was mounted 10 cm from the sample within the heating stage to measure the scattering pattern.

Samples for WAXD, SAXS, TEM and SEM were compression moulded between PTFE films into plaques approximately 0.05 × 5 × 10 cm. All WAXD experiments were performed on a Nicolet diffractometer operating at 40 kV and 30 mA and equipped with a STOE Bragg–Bernatto type goniometer. Cu-K_α X-rays (1.54 Å) were passed through a graphite monochromator before final collimation. Data were collected at 0.1° increments between the scattering angles of 10–35°. For all runs two plaques were stacked to optimize thickness. Data collection and analysis was performed by the Siemens Polycrystalline Software Package.

SAXS measurements were performed using a Siemens Kratky camera system with an M. Braun position-sensitive detector from Innovative Technology, Inc. A Philips model PW 1729 tabletop generator was used. For all experiments the generator was set to 40 kV and 20 mA using the Cu-K_α X-ray (1.54 Å). Lead stearate was used for angular calibration and Lupolen for absolute intensity calibration.

TEM samples were prepared from the same films that were used for WAXD and SAXS. Samples were

microtomed at −20°C using a Reichert–Jung ultracut E43 ultramicrotome equipped with a diamond knife. Samples were cut to a thickness of 500–1000 Å and were chemically stained with ruthenium tetroxide (RuO_4)[22] by suspending them over a 0.5% solution of RuO_4 for 30–60 min. All TEM experiments were performed on a Philips IL 420T STEM with an acceleration voltage of 100–120 kV.

After running WAXD and SAXS experiments on the compression-moulded plaques they were cut into small pieces and etched using a permanganic acid permanganate solution[23]. The concentrated solution consisted of 0.5 g of K_2MnO_4 dissolved in 20 ml of 85% H_3PO_4 diluted with 20 ml H_2O; the dilute solution differed from the concentrated solution in that it was diluted to a volume of 120 ml. Following etching, all samples were sputter coated with gold in a Bio Rad E5400 high-resolution SEM sputter coater to a thickness of approximately 210 Å. A Cambridge Instruments Stereoscan 200 scanning electron microscope with an operating voltage of 25 kV was used for all scanning electron microscopy experiments.

Rheological studies

Samples for rheological experiments were compression moulded into 25.4 × 1 mm discs. All measurements were performed on an RMS 800 shear rheometer. For all samples, melting was completed by the time the temperature had reached 240°C. Samples were held at 240°C for 10 min prior to rheological testing. During this period, no differences were noted in complex viscosity. Strain sweeps were performed from 1% to 10% strain at 240°C, frequency sweeps from 0.1 to 100 radians per second at 240°C and temperature sweeps from 260°C to 200°C at 10 radians per second. Temperature sweeps were performed at a rate of 10°C min^{-1} in order to obtain viscosity measurements in the supercooled melt before the onset of crystallization. The strain rate of 10 radians per second was chosen to keep torques high enough to be measurable in the branched systems, which showed substantially reduced melt viscosities compared to linear samples of comparable molecular weight.

Bulk crystallization rate

A Perkin–Elmer DSC-4 and a Seiko DSC 210 were used to obtain bulk crystallization information. In both cases, indium was used for temperature calibration. After being held in the melt for 10 min all samples were isothermally crystallized in 20 mg aluminium pans. Samples were held in the melt in order to correlate the thermal history of d.s.c. experiments with that of experiments described earlier. Isothermal crystallization experiments were performed in the temperature range of 190–207°C. The lower limit of 190°C was dictated by the maximum cooling rate available, for achievement of temperatures below 190°C before the onset of crystallization. The upper limit was set by the long induction times before the onset of crystallization and the resulting problems with thermal stability and reduced signal-to-noise ratio. Due to the inability to quench samples from the melt rapidly but controllably, crystallization data from the diffusion-controlled crystallization temperature range were not obtainable.

DATA ANALYSIS

SALS

Spherulitic structure, evident in many polymers, generally results in a (SALS) pattern under cross-polarized light with fourfold symmetry. This pattern is known as the 'four-leaf clover'[24]. At the intensity maximum of each lobe, the following relationship is satisfied:

$$4.09 = 4\pi R \sin(\Theta_{max}/2)/\lambda_m \quad (1)$$

In this case R is the average spherulite radius, Θ_{max} is the scattering angle at which an intensity maximum is observed and λ_m is the wavelength of light in the material. Since Θ_{max} is easily obtained from photographic measurements, SALS is a rapid means of determining average spherulite size.

WAXD

Wide angle X-ray diffraction was primarily used to determine whether any structural differences or differences in crystallinity were observable as a function of branch-point functionality. WAXD also allowed for an independent determination of absolute crystallinity which could later be correlated with heat of fusion measurements obtained by d.s.c.

The classical method of Hermans and Weidinger[25] was used to determine absolute crystalline fraction in each of our three samples. This procedure involves the separation of X-ray scattering intensities into amorphous and crystalline components. Since our samples are homogeneous and isotropic, the crystalline fraction is the ratio of integrated intensity beneath the crystalline peaks over the integrated total intensity. The above procedure is based upon the assumption that the crystalline peaks can be deconvoluted from the amorphous scatter. The method of peak deconvolution that we selected was utilized by Vonk to determine absolute crystallinity in a number of polymers[26]. It involves obtaining an amorphous scattering profile and subtracting the lineshape from the amplitude and baseline corrected total scattered intensity. The experimental method of peak resolution is outlined in *Figure 2*. Since no WAXD heating stage was available at our facility, and nylon-6

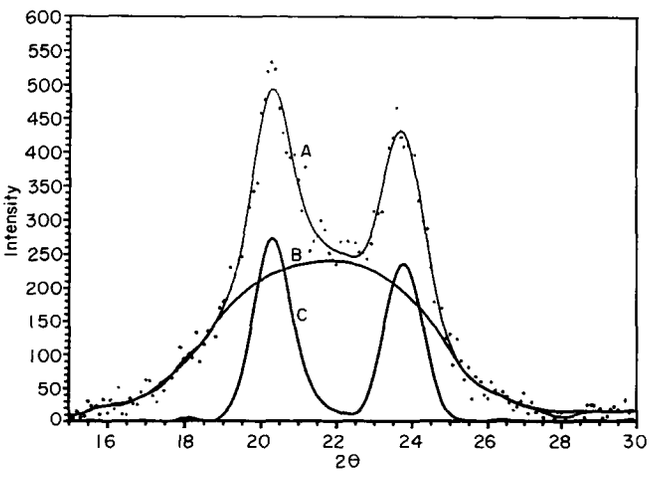

Figure 2 Resolution of WAXD data into amorphous and crystalline components. A – baseline corrected raw data points and Fourier-fitted curve; B – baseline and amplitude-corrected amorphous scattering profile; C – resolved crystalline peaks

could not be adequately quenched to obtain an amorphous standard, the amorphous scattering profile of nylon-6 was obtained from an earlier study on linear nylon-6[27]. Since no crystallographic differences were observable between our samples as a function of branch-point functionality, it was assumed that the linear nylon-6 standard was a valid standard for all branching architectures investigated.

The method of Hermans and Weidinger may underestimate the absolute crystallinity by 10% or more due to its neglect of spatial and thermal disorder as well as amplitude corrections as a result of atomic scattering and structure factors[28]. Although the effects of thermal diffuse scattering were not taken into account in this study, Ruland[29] has shown that in polymers containing interchain hydrogen bonding the effects of thermal disorder are not as significant as in polymers lacking strong secondary interactions. Preliminary calculations considering the effects of atomic scattering factors as well as structure factors suggest that the systematic error introduced by using the method of Hermans and Weidinger is less than 5%, on the order of our experimental uncertainty.

Thermal analysis

D.s.c. (percentage crystallinity). Percentage crystallinity was determined from calorimetric data by integrating the entire region under the melting endotherm to obtain heat of fusion as a function of temperature. A molar heat of fusion of 21 ± 2 kJ/mol$_{\text{Rpt.unit}}$ for nylon-6 (100% crystalline material) was obtained by averaging several values obtained in earlier studies[30]. The following equation was used to determine percentage crystallinity:

$$\%\ \text{xtal} = (\Delta H_{\text{measured}}/\Delta H_{100\%\ \text{xtal.}}) * 100\% \qquad (2)$$

D.s.c. (crystallization kinetics). The overall rate of bulk crystallization can often be analysed in terms of the Avrami equation[31]:

$$X_c(t) = 1 - e^{-Kt^n} \qquad (3)$$

where $X_c(t)$ is the volume fraction of crystals at time, t, after the onset of crystallization. Often at low values of supercooling an induction period may occur before the onset of crystallization. K is a rate constant including temperature-dependent terms involving diffusion, growth and nucleation density; and n, the Avrami exponent, is a constant depending on the types of processes occurring during nucleation and growth.

Taking the double logarithm of equation (3) we obtain:

$$\ln[-\ln(1 - X_c(t))] = \ln K + n \ln t \qquad (4)$$

Thus a plot of the double logarithm of amorphous content as a function of ln(time), a classical Avrami plot, gives a straight line with slope n and calculated intercept ln K.

An alternative method of determining crystallization parameters involves the use of crystallization half-time. In this case the entire area under the crystallization exotherm represents a normalized crystalline content of unity. On a normalized basis the crystallization half-time, $t_{1/2}$, is defined as the time at which the normalized crystalline content is 0.5. From a graph of normalized crystalline content *versus* ln(time) one may determine the Avrami exponent, n, from the slope at $t = t_{1/2}$, $S_{t1/2}$.

Taking the logarithm of equation (3) at $t = t_{1/2}$ one obtains[32]:

$$K = \ln(2)/t_{1/2}^n \qquad (5)$$

The slope of the curve $(1 - X_c(t))$ as a function of ln(time) may be written as:

$$S = t^*[\delta(1 - X_c(t))]/\delta t \qquad (6)$$

From equation (3) $\delta[1 - X_c(t)]/\delta t$ may be calculated:

$$\delta[1 - X_c(t)]/\delta t = -Knt^{n-1}e^{-kt^n} \qquad (7)$$

at $t = t_{1/2}$:

$$S_{t1/2} = n \ln(2)/2 \qquad (8)$$

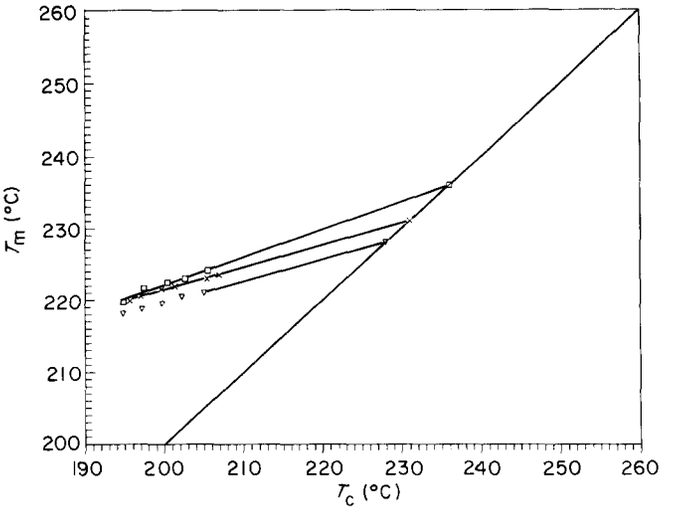

Figure 3 Effect of branch-point functionality on Hoffman Weeks plots: □, $f = 2$, $T_m = 236$°C; ×, $f = 3$, $T_m = 231$°C; ▽, $f = 6$, $T_m = 228$°C

RESULTS AND DISCUSSION

The effect of branch functionality on equilibrium melting points, T_m^0, was determined using the method of Hoffman and Weeks[33]. *Figure 3* shows the data used to determine the equilibrium melting points as a function of branch point functionality while keeping *DP* nearly constant. This method gives equilibrium melting points of 236°C for linear nylon-6, 231°C for the three-arm nylon-6 and 228°C for the six-arm nylon-6. Melting points observed by d.s.c. were consistently lowered as a function of increasing branch-point functionality (*Figure 4*). A similar depression of melting points observed by d.s.c. had been noted by Mathias and Sikes on a different star-branched nylon-6 system[14,15], but the equilibrium melting points were not determined for their polymers.

The origin of the depression of equilibrium melting points can be related to the nature of the lamellar crystals formed in the branched *versus* linear systems. The enthalpy of formation for a chain-folded lamellar crystal is[34]:

$$\Delta H_{\text{crystal}} = 4xl\sigma + 2x^2\sigma_e - x^2l(\Delta f) \qquad (9)$$

In this case, x is the lateral dimension of the crystal, l is the lamellar thickness, σ is the lateral surface energy, σ_e is the fold surface energy and Δf is the bulk-free energy of fusion. For crystals with $x \gg l$ it can be shown that the melting temperature may be estimated by[34]:

$$T_m = T_m^0[1 - 2\sigma_e/(\Delta h_f)l] \qquad (10)$$

Equation (10) predicts a melting point depression of

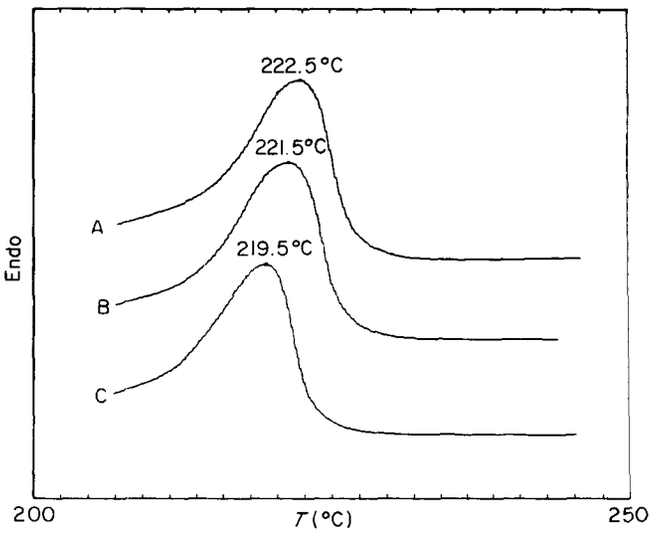

Figure 4 Effect of branch-point functionality on d.s.c. melting endotherms for samples isothermally crystallized at 200°C. A – linear nylon-6; $T_m = 222.5$°C; B – three-arm nylon-6; $T_m = 221.5$°C; C – six-arm nylon-6; $T_m = 219.5$°C

$(2T_m^0\sigma_e/\Delta hl)$ for a thin lamellar crystal below that of an infinitely thick crystal. Since it will be shown later that the average thickness of lamellar crystals of nylon-6 is not greatly affected by branch-point functionality, the data in *Figure 3* suggest that the ratio $(\sigma_e/\Delta h)$ for crystals of star-branched nylon-6 is less than that for linear nylon-6 by 26% for six-arm nylon-6 and 22% for three-arm nylon-6.

An expected result of the entropic constraint imposed on the branched molecules would be to promote an increased equilibrium melting point for crystals of branched polymers when compared to their linear counterparts. Since the observed trend is in the opposite direction, the effect of the additional entropic constraint appears to be minimal. The observed depression of melting points may be attributed to differences in bulk enthalpy of fusion and greater fold surface energies in crystals of branched polymers due to local defects. The enthalpy of formation of a crystal will be decreased if bulky branch-points and end groups are included within or near the surface of a crystal. End groups lack the spatial symmetry necessary to pack into the crystal lattice, and, noting that the chemical structure of the branch-points is substantially different than that of nylon-6, it is unlikely that such a structure can pack into lamellar crystals. As the concentration of branch-points and end groups increases, the equilibrium melting point of the polymer crystals should decrease.

In order to substantiate the above arguments, the equilibrium melting point of six-arm nylon-6 with a considerably higher DP (1150) was determined. Since the concentration of branch-points and end groups in this higher molecular weight system is decreased compared to the lower molecular weight six-arm system by a factor of four, the equilibrium melting point should be nearer to that of the linear system. Indeed, the equilibrium melting point of star-branched nylon-6 with $DP = 11\,500$ was determined to be 232°C, 6°C higher than six-arm nylon-6 with $DP = 270$. Thus as an effect of branching, the melting point depression in our system appears to be directly correlated to changes in bulk crystallization enthalpy and steric interactions, resulting in higher fold surface energy. Recently Roland and Buckley[35] have used the above arguments to attribute changes in the thermodynamic stability, i.e. equilibrium melting point, of polytetrahydrofuran networks to crosslink density. On a local scale the branch-points in star-branched nylon-6 behave much like a crosslink in terms of decreasing the thermodynamic stability of a crystal.

Data from isothermal crystallization experiments were put in the format for crystallization half-time analysis (*Figure 5*) as well as classical Avrami analysis (*Figure 6*). *Figure 5* shows plots of the normalized crystalline content of linear nylon-6, three-arm nylon-6 and six-arm nylon-6 as a function of ln(time). From these data and equations (5) and (8) the Avrami exponents, n, and rate constants, K, were determined as a function of temperature (*Figures 7* and *8*). Analysis on the Avrami plots using equation (4) (*Figure 6*) yielded the n and K values from the slope and the log of the intercept (*Figures 9* and *10*). In experiments where an induction period was observed, star-branched nylon-6 showed substantially shorter induction periods before the onset of crystallization when compared to the linear polymer crystallized at the same temperature.

Both analysis methods revealed a decrease in the Avrami exponent with decreasing temperature in all samples. Earlier studies on the crystallization kinetics of linear nylon-6 revealed Avrami exponents that ranged from 2 to 3 for isothermal crystallization temperatures ranging from 150°C to 190°C[11,13]. Magill noted through microscopy and optical depolarization experiments that heterogeneous nucleation was prominent at temperatures below 190°C, but at temperatures above 190°C sporadic, homogeneous nucleation became evident and Avrami exponents approaching 4 were observed[13]. No significant changes in the Avrami exponent as a function of branch-point functionality were evident. However, Avrami exponents showed a definite increase at temperatures above 197°C. Avrami exponents had an average value of 2.8 in the temperature range of 190–197°C; for temperatures above 197°C the average Avrami exponent increased to about 4. Theoretically, this increase in Avrami exponent may correspond to the transition from heterogeneous nucleation with three-dimensional spherulitic growth to homogeneous nucleation with three-dimensional spherulitic growth.

The effect of branch-point functionality on crystallization half-times is shown in *Figure 11*. Plotting crystallization half-times as a function of supercooling eliminates the observed effect of branching on equilibrium melting point that would be present if these values were plotted as a function of crystallization temperature. Hser and Carr[16] observed that star-branched polyethylene showed significantly lower crystallization half-times as a

Table 2 Coupling parameters as measured from temperature dependence of shear viscosity

Sample designation	Branch-point functionality	M_w	$\frac{\Delta \log \eta}{\Delta(T^{-1})}$	n_f
Linear	2	29 000	3290	0.39
Three-arm	3	36 000	3120	0.35
Six-arm	6	42 000	2720	0.26
Six-arm	6	105 000	3290	0.39

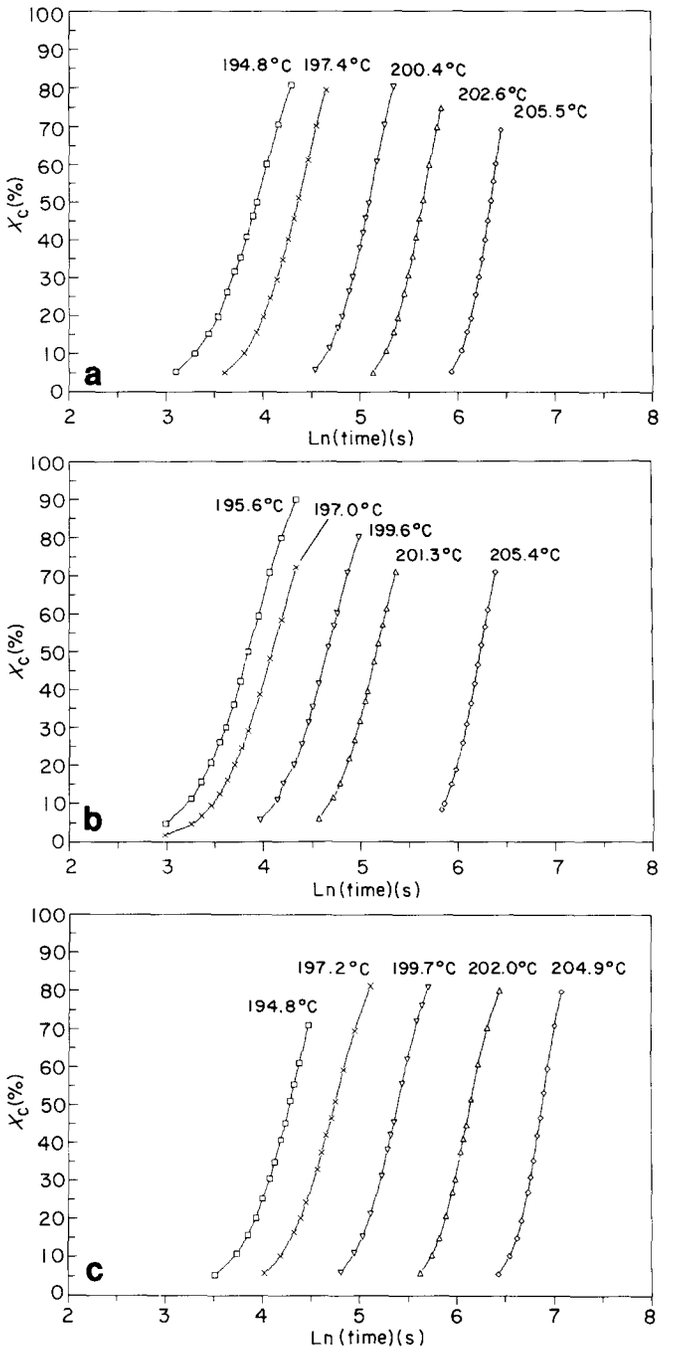

Figure 5 Normalized crystalline content *versus* time. (a) Linear nylon-6, (b) three-arm nylon-6, (c) six-arm nylon-6

function of supercooling compared to linear polyethylenes of equivalent molecular weight. A similar but less pronounced effect is seen in the nylon-6 utilized in this study. The crystallization half-times for the linear polymer are nearly twice those observed for the six-arm system at equivalent supercooling. The branched systems also appear to display an increased dependence of crystallization half-times on supercooling relative to the linear polymer; this increased supercooling dependence is also consistent with data obtained by Hser and Carr. Decreased crystallization half-times are desirable for most applications since a higher degree of absolute crystallinity can be obtained in less time with equivalent supercooling, other factors being equivalent.

When discussing the effects of chain branching on crystallization it is important to consider that branching may have two counteracting effects on the rate at which polymer chains may be deposited on the surface of a growing lamellar crystal. For most polymers of relatively low molecular weight, the dominant mode of diffusion is reptation. de Gennes[36] has shown that branching tends to increase reptation times by a factor that is exponential in the number of entanglements per branch compared to the power law dependence observed for linear chains. A counteracting effect arises from the fact that branched chains tend to have a much smaller radius of gyration than linear chains of similar molecular weight. Reduced hydrodynamic volume is evident in star-branched polymers through reduced intrinsic viscosity[5,14,15]. Branched chains, thus, tend to be more compact and form entanglements with fewer neighbours than linear polymers of equivalent

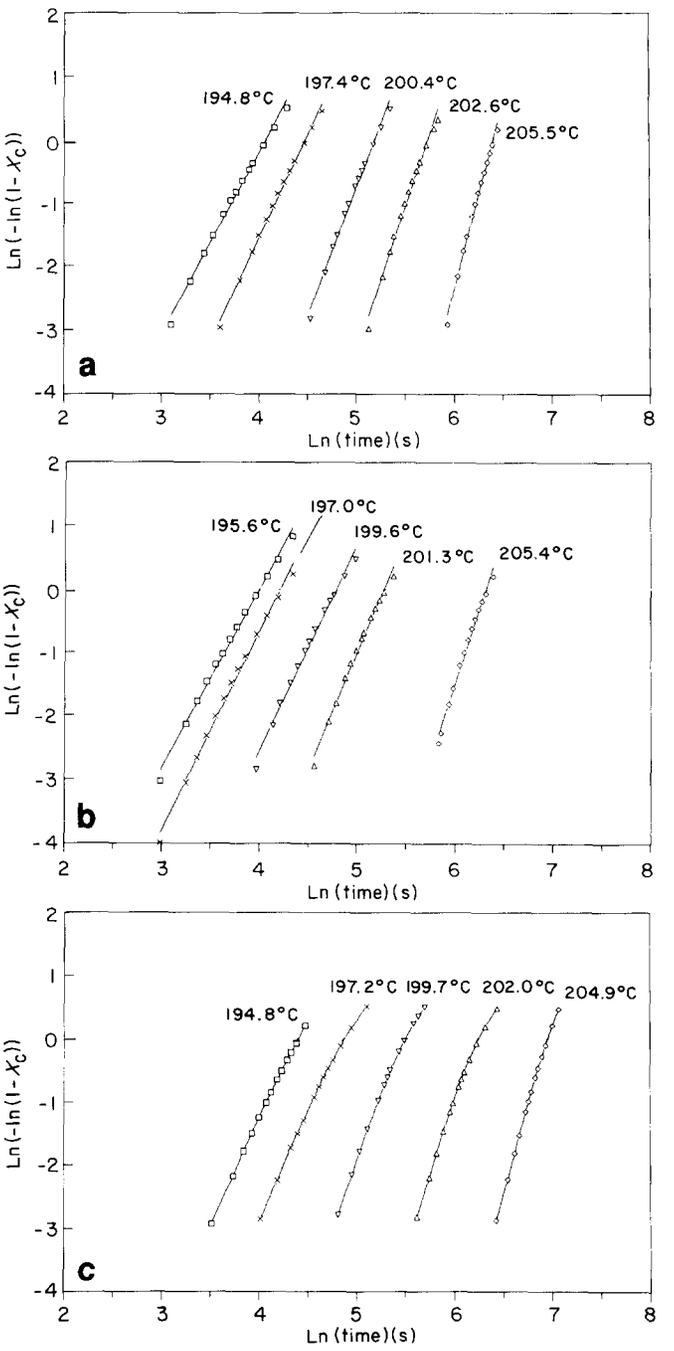

Figure 6 Avrami plots. (a) Linear nylon-6, (b) three-arm nylon-6, (c) six-arm nylon-6

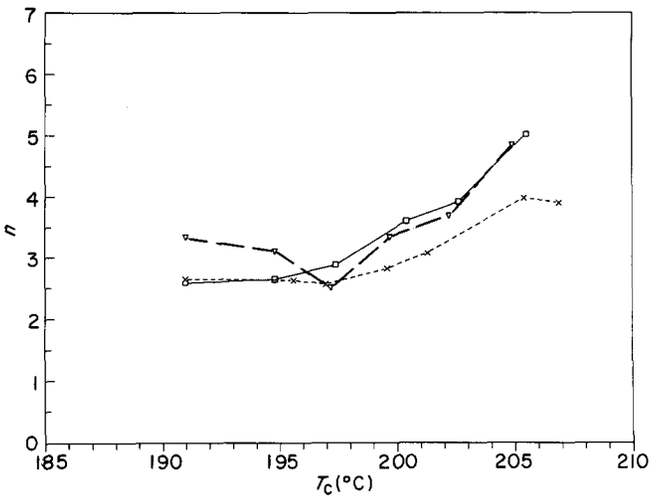

Figure 7 Avrami exponent, n, *versus* T_c: effect of branch-point functionality as determined by crystallization half-time analysis: □, $f=2$, $DP=270$; ×, $f=3$, $DP=300$; ▽, $f=6$, $DP=270$

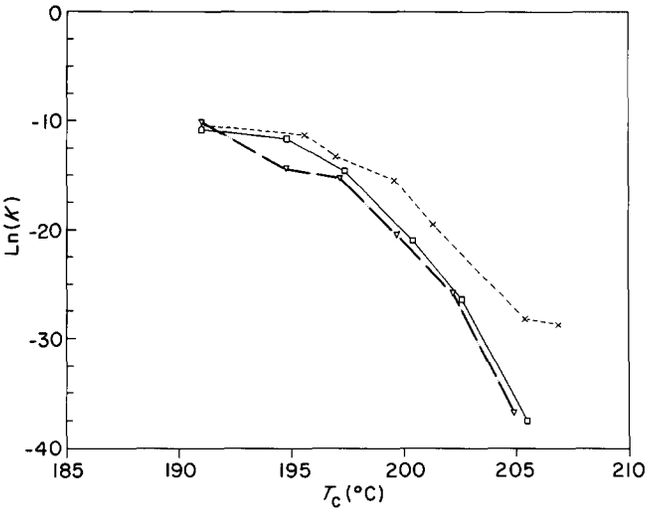

Figure 10 Rate constant, K, *versus* T_c: effect of branch-point functionality as determined by classical Avrami analysis. Symbols as in *Figure 7*

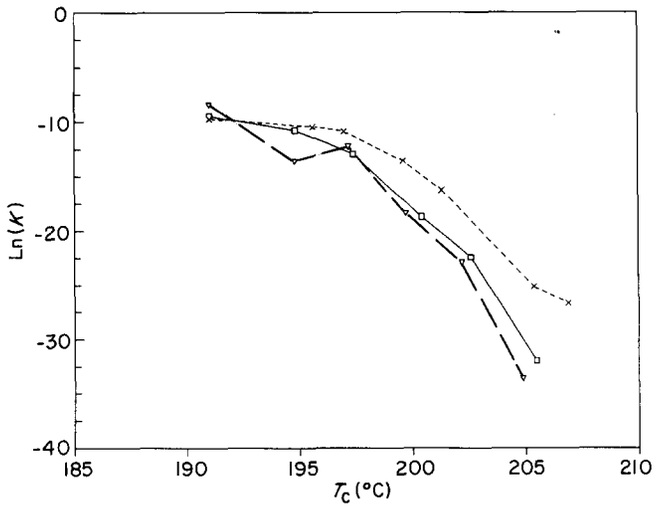

Figure 8 Rate constant, K, *versus* T_c: effect of branch-point functionality as determined by crystallization half-time analysis. Symbols as in *Figure 7*

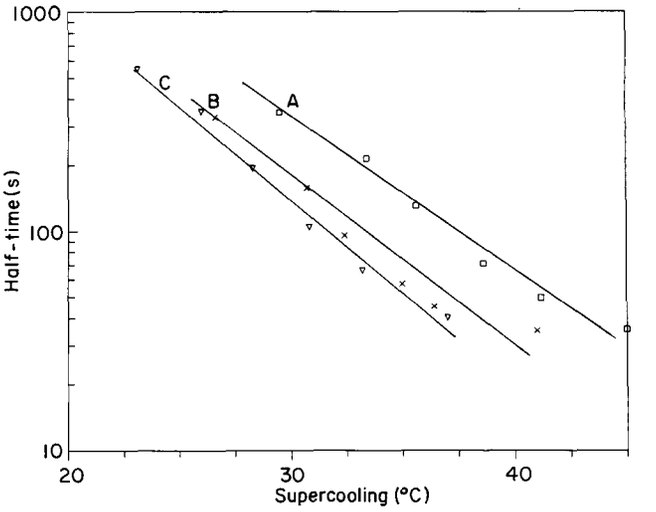

Figure 11 Effect of branch-point functionality on crystallization half-times *versus* supercooling. A – linear nylon-6, □, B – three-arm nylon-6, ×, C – six-arm nylon-6, ◇. Symbols as in *Figure 7*

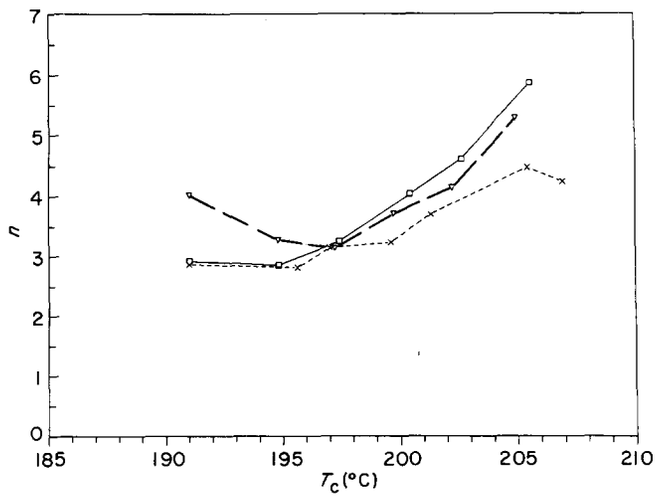

Figure 9 Avrami exponent, n, *versus* T_c: effect of branch-point functionality as determined by classical Avrami analysis. Symbols as in *Figure 7*

molecular weight. Further complicating the picture are the considerations that constraint release and coupling parameters, a measure of the extent to which the average polymer molecule is entangled with its neighbours, may vary considerably depending on branch-point functionality. Ngai *et al.*[37] have shown that coupling parameters may vary considerably, depending on branch-point functionality. Lodge *et al.*[38], on the other hand, have shown that coupling parameters for star polymers with arm lengths well above the entanglement length are nearly constant as a function of branch-point functionality. Viovy *et al.*[39] as well as Roovers[40], have proposed that constraint release in polymer melts may vary greatly as a function of macromolecular topology. However, the exact nature of this process in non-linear systems is still not well understood.

In order to measure the effects of star-branching on diffusion times and entanglement coupling, viscosity *versus* temperature sweeps were performed from 260°C to 200°C (*Figure 12*). By performing a downward

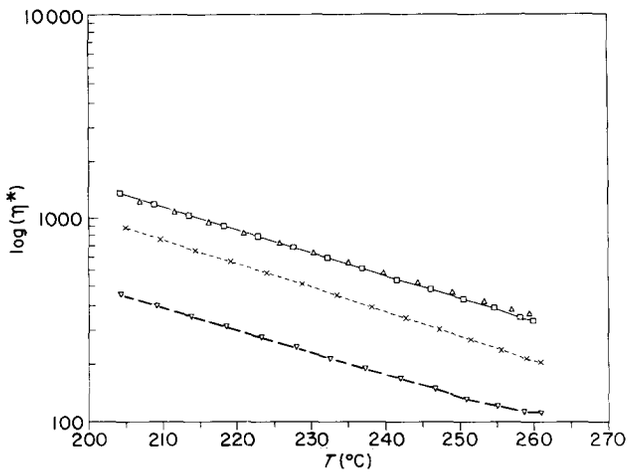

Figure 12 Effects of branch-point functionality on complex viscosity; temperature sweeps at 10 rad s^{-1}: □ – Linear nylon-6, $DP=270$; $\langle M_n\rangle=30\,900$, × – three-arm nylon-6, $DP=800$; $\langle M_n\rangle=31\,500$, △ – six-arm nylon-6, $DP=1150$; $\langle M_n\rangle=130\,000$, ▽ – six-arm nylon-6, $DP=270$; $\langle M_n\rangle=30\,900$

temperature sweep at 10°C min^{-1} viscosities of the supercooled melt could be measured before the onset of crystallization. As suggested by crystallization half-time measurements, viscosities of the supercooled melts were greatly reduced as a function of increasing branch-point functionality. The behaviour of both linear and star-branched nylon-6 may be explained by the coupling model for entangled polymer melts. At temperatures well above the glass transition the viscosity of a polymer may be represented by[41]:

$$\eta \equiv M^{\alpha}[\zeta(T)] \equiv M^{\alpha}[\zeta_0(T)]^{(1/(1-n(f))} \tag{11}$$

where the monomeric friction factor, $\zeta(T)$, can be expressed in the Arrhenius form as:

$$\zeta(T) = Ce^{E_a/[(1-n(f))RT]} \tag{12}$$

where $n(f)$ is the coupling parameter. Ngai and Plazek[41] have shown that the primitive flow activation energy, E_a, of polymers is more a function of bond rotational energies than topology. Therefore, the coupling parameter, $n(f)$, of linear or star-branched systems may be calculated from the temperature dependence of viscosity[41]. A plot of $\ln(\eta)$ *versus* $1/T$ has slope $E_a/(1-n(f))R$. Since E_a is essentially a function of bond rotational energy, independent of topology, $n(f)$ may be determined. The value of E_a was estimated from that of a methylene group in linear polyethylene as determined by Ngai and Plazek[41], since this is the most flexible link in the nylon-6 chain. The true value of E_a in nylon-6 is likely to be somewhat larger than that for the methylene linkage due to the presence of amide linkages.

In this way the coupling parameters of the three-arm and linear polymer with molecular weight (*ca* 30 000) were found to be nearly identical as predicted by Lodge *et al.* (*Table 2*). However, the coupling parameter of the six-arm system was found to be reduced by nearly a factor of two when compared to that of the linear system. When similar measurements were performed on a six-arm nylon-6 with four times the molecular weight, the coupling parameter was found to agree with the linear value.

The average molecular weight between entanglements, M_e, in nylon-6 is approximately 5000 (ref. 42). From this value we would expect an average of six entanglements per molecule for the samples in this system with weight average molecular weight of 30 000. However, the weight average molecular weight of each arm in the six-arm system is only 7000, very close to the critical length for entanglements, $(M_w/M_e)\approx 1$. Since the weight average molecular weight per arm is so close to the critical molecular weight between entanglements, it is expected that only about half of the arms in this system are effectively entangled with neighbours due to the distribution of arm lengths and lengths between entanglements. The end result is that the coupling parameter in this system should be significantly reduced compared to that of the linear polymer. This hypothesis is further verified by the fact that the coupling constant increases for the six-arm stars when the molecular weight of the arms increases above the average critical length for entanglements, $(M_w/M_e)\gg 1$ (see *Table 2*).

Ngai and Plazek have shown that in entangled polymer melts the zero-shear viscosity of branched polymers may be substantially greater than that for the linear counterpart due to the exponential dependence of viscosity on the number of entanglements per arm in branched polymers. This study, however, suggests that if the number of entanglements per arm is kept low, melt viscosities of branched polymers may be reduced substantially when compared to their linear counterpart. Due to the exponential dependence of melt viscosity on the number of entanglements in branched polymers *versus* the power law dependence for linear polymers, the effects of regular branching on the viscosity of a polymer is dependent on the ratio (M_w/M_e). If this ratio is kept low, the effect of star branching is to reduce reptation times; when this ratio becomes large[43,44], i.e. $(M_w/M_e)_{arm}>4$, the rapidly increasing exponential dependence produces slowed reptation times and thus greater viscosities. As a consequence, the increased molecular weight dependence on reptation times for branched polymers means that molecular weight and polydispersity must be more precisely controlled in order to produce consistent melt viscosities for industrial applications.

The self-diffusion coefficient for a polymer melt may be represented in an Arrhenius form analogous to equation (12) above:

$$D_f = Ce^{-E_a/[(1-n(f))RT]} \tag{13}$$

The average terminal relaxation time of the polymer melt may thus be expressed as[39]:

$$\langle\tau\rangle = \langle R_g^2\rangle/D_f \tag{14}$$

For high molecular weight, flexible polymers, the effects of regular star-branching on the average radius of gyration may be approximated by[45]:

$$\langle R_{g,f'}^2\rangle/\langle R_{g,f}^2\rangle = (3f'-2)*f'^2/(3f-2)*f'^2 \tag{15}$$

where f and f' are branch-point functionalities of polymers with equivalent molecular weight. In order for star-branching to slow terminal relaxations, the coupling parameter must be large enough to offset the effect of reduced hydrodynamic volumes. This may only occur at molecular weights well above the critical molecular weight for entanglement, M_e.

Star branching reduces reptation times in nylon-6 in the range of molecular weights used in this study. This reduction in reptation times is responsible for the greatly reduced melt viscosities of star-branched nylon-6

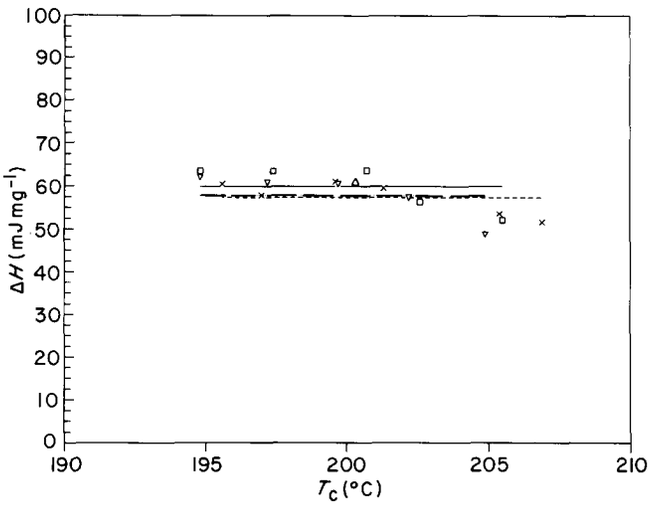

Figure 13 Effect of branch-point functionality on the heat of melting *versus* temperature. □, linear nylon-6, $\langle M_n \rangle = 30\,900$; ×, three-arm nylon-6, $\langle M_n \rangle = 31\,500$; ▽, six-arm nylon-6, $\langle M_n \rangle = 30\,900$; △, six-arm nylon-6, $\langle M_n \rangle = 130\,000$

compared to its linear counterpart with comparable molecular weight; even for the six-arm stars with high molecular weight the melt viscosity was reduced to that of the linear polymer of much lower number average molecular weight. Due to reduced terminal relaxation times, polymer chains may more easily diffuse onto the surface of growing lamellar crystals. Assuming that spherulitic growth and nucleation are otherwise identical, the result of reduced reptation times is to also reduce crystallization half-times as a function of supercooling for nylon-6 with increasing branch-point functionality. The exact nature of spherulitic nucleation and growth in linear *versus* star-branched polymers will be discussed later in this paper.

It can be argued that the cause of the lower equilibrium melting points in star-branched nylon-6 is the local effect that a branch-point has on the thermodynamic stability of crystal. A branch-point cannot be packed into a crystal lattice without causing a defect and topologically constraining its neighbours. Inclusion of such defects might also tend to reduce the absolute crystallinity measured by X-ray and d.s.c. In each of the polymers investigated in this study the initiator chemistry was somewhat different from that of nylon-6. Therefore even in the linear system, initiated by a difunctional amine, it is unlikely that this chemically different portion of the polymer chain could pack into a crystal lattice; although the topological constraints in this case would be negligible.

Values of the heat of melting as a function of crystallization temperature were obtained by integration under the entire melting endotherm. These values were then used in combination with equation (2) to determine absolute crystallinity. *Figure 13* shows the effect of branch-point functionality as well as temperature on measured heat of melting. There appears to be a slight reduction in measured heat of melting of crystals of star-branched nylon-6 compared to crystals of linear nylon-6. This reduction may be attributed to higher fold surface energies of lamellar crystals or a decrease in bulk crystalline enthalpy due to inclusion of bulky branch-points at or near the surface of such crystals, since no significant change in absolute crystallinity was measured by WAXD (*Table 3*). The reduced heat of melting for crystals of star-branched nylon-6 relative to linear nylon-6 is consistent with depressed melting points for star-branched nylon-6. The trend towards lower values of heat of melting at high T_c is likely due to the fact that these crystals were not held at the crystallization temperature long enough for secondary crystallization to be completed.

In this system both chain ends and branch-points may cause crystalline defects. As molecular weight is kept constant and branch-point functionality increases, the concentration of both types of defects in a crystal increases. The melting point of a crystal may be described by:

$$T_m^0 = \Delta H_{fus.}/\Delta S_{fus.} \quad (16)$$

where $\Delta H_{fus.}$ is the bulk enthalpy of fusion, and $\Delta S_{fus.}$ is the bulk entropy of fusion. If the entropic effect of the additional constraint in a star-branched system were significant, the expected result would be an increase in equilibrium melting point. Since the contrary is observed, it is apparent that enthalpic effects are much more significant. The inclusion of a defect such as an end group or branch-point at or near the surface of a crystal lattice would be expected to reduce the enthalpy of fusion of such a crystal. Heat of fusion measurements were performed on six-arm nylon-6 with $DP = 1150$ in order to determine if the lower concentration of end groups and branch-points in this system would lead to a heat of fusion closer to that of linear nylon-6. However, the detected difference in heat of fusion was not beyond experimental uncertainty (60.4 mJ mg^{-1} for the sample with $DP = 270$ *versus* 60.7 mJ mg^{-1} for the sample with $DP = 1150$). The results obtained while keeping molecular weight constant, and changing branch-point functionality alone, are enough to suggest that bulk heats of fusion of crystals containing star-branched polymers are indeed reduced compared to their linear counterparts.

Depressed equilibrium melting points as well as lowered heats of fusion in crystals containing star-branching is consistent with the greater number of possible defects within crystals of star-branched polymers. However, no appreciable differences between the crystal structure of linear *versus* branched systems were observed by WAXS (*Figure 14*). Absolute crystallization measurements by WAXS and d.s.c. reveal only small differences for samples with an identical thermal history – see *Table 3*. Since the observed depression of equilibrium melting points is small, the effects of star-branching may lie at the limits of sensitivity of our instruments. Additionally, WAXS measurements are less sensitive to defects at the edges of lamellar crystals and corresponding increases in fold surface energy due to steric interactions. The agreement between absolute crystallinity measured by WAXS and d.s.c. suggests that the value used in this study

Table 3 Effect of branch-point functionality on the absolute crystallinity determined by WAXD and d.s.c.

	% Crystallinity	
Sample	D.s.c. ± 1%	WAXD ± 2%
Linear	33	31
Three-arm	31	30
Six-arm	31	31

for the molar heat of fusion of nylon-6 (21 kJ $mol_{Rpt.unit}$) is an accurate value.

Since the values of the bulk crystallization constant, K, contain information about growth rate as well as nucleation density, it was imperative to see whether any differences in morphological features, i.e. nucleation density, were evident. Morphological studies were also needed to confirm our assumptions about nucleation and growth processes based on the Avrami exponent.

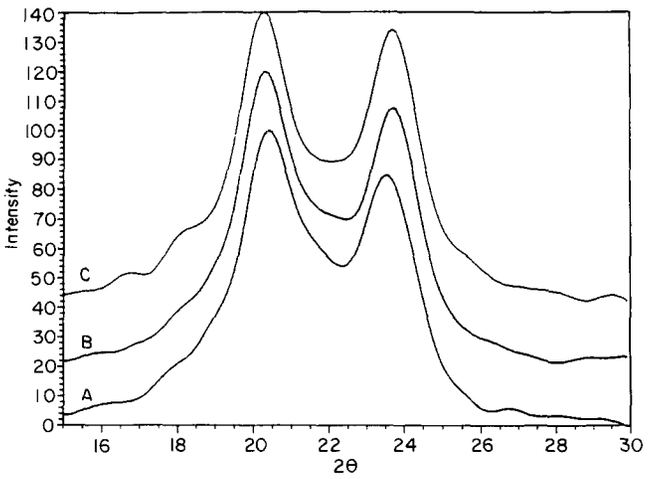

Figure 14 Wide angle X-ray diffraction patterns of samples crystallized at 200°C. A – linear nylon-6, B – three-arm nylon-6, C – six-arm nylon-6

Optical polarized microscopy measurements, summarized in *Figure 15*, revealed changes in nucleation density and average spherulite size as a function of temperature. Average spherulite diameter for specimens crystallized at 200°C were on the order of 10 μm, apparently with a rather broad distribution of spherulite sizes. Optical polarized microscopy also revealed a trend towards slightly smaller spherulites in the three-arm system. The size of the spherulitic structures, however, was difficult to estimate from OPM measurements.

Small angle light scattering, H_v, patterns were used to obtain a more accurate indication of average spherulite radius as a function of branch-point functionality and temperature. These experiments revealed Θ_{max} values in the 3–9° range, indicating an average spherulite radius of the order of 2–5 μm – see *Figure 16*. The average angle at which the maximum in the light scattering pattern, $\Theta_{max.}$, occurred did not vary appreciably as a function of branch-point functionality except for the case of the three-arm system, which tended to show a consistently higher value of Θ_{max}. Since six separate samples were run to verify the reproducibility of results, it is believed that the spherulites in the three-arm system were statistically slightly smaller than those in the linear and six-arm systems. The results of SALS experiments are provided in *Table 4*. In the cases where two values are given, the high and low values of several experiments are shown.

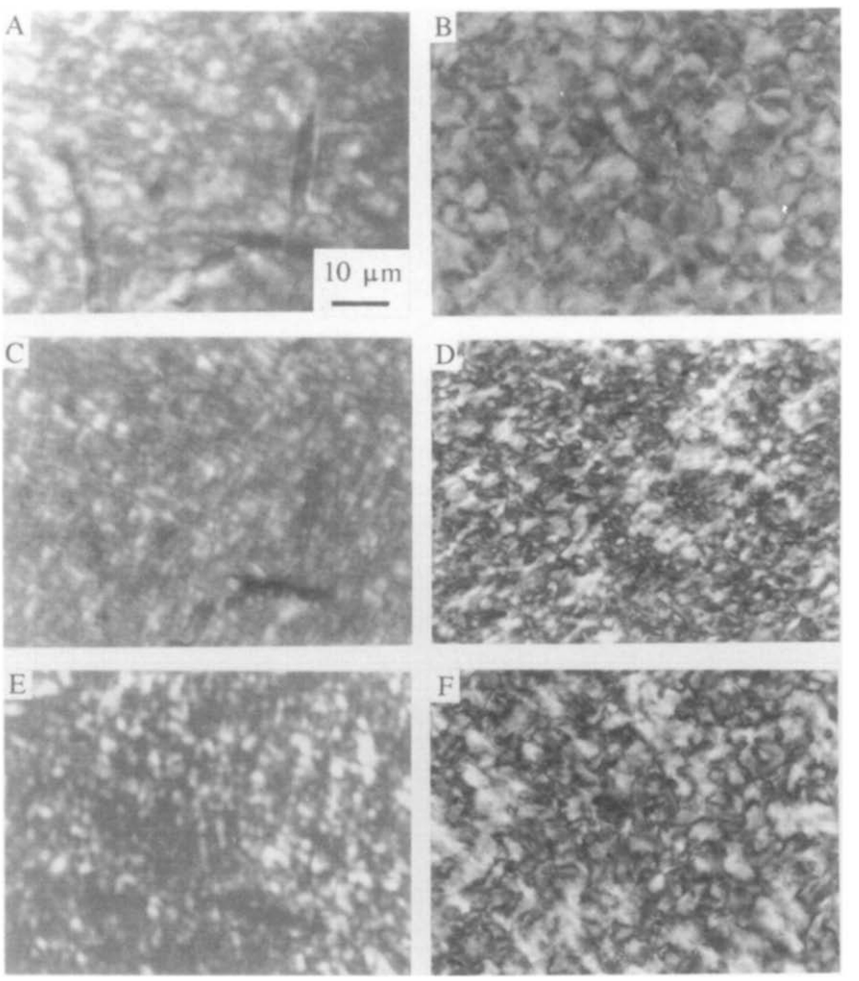

Figure 15 Optical micrographs of star-branched nylon-6 between cross-polarizers. A, B – linear, crystallized at 191°C and 200°C, respectively, C, D – three-arm, crystallized at 191°C and 200°C, E, F – six-arm, crystallized at 191°C and 200°C

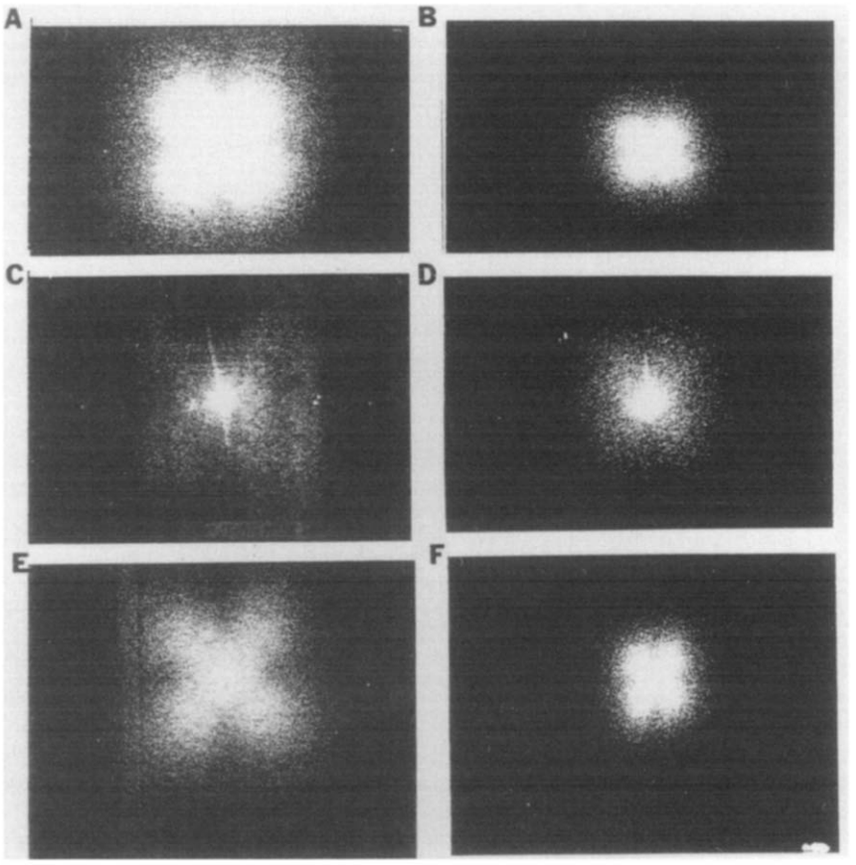

Figure 16 H_v SALS patterns obtained from star-branched nylon-6. A, B – linear, crystallized at 191°C and 200°C, respectively, C, D – three-arm, crystallized at 191°C and 200°C, E, F – six-arm, crystallized at 191°C and 200°C

Table 4 Results of H_v SALS experiments

Sample	Θ_{max}	Spherulite radius (μm)
(a) Samples crystallized at 191°C		
Linear	5.7	2.7
Three-arm	8.5	1.8
Six-arm	5.7	2.7
(b) Samples crystallized at 200°C		
Linear	2.9	5.4
	4.3	3.6
Three-arm	4.3	3.6
	5.7	2.7
Six-arm	2.9	5.4
	4.3	3.6

Scanning electron microscopy was used to obtain further detail of the morphological features of the star-branched nylon system. By varying etching time and etchant concentration, differences between bulk and surface morphology could be better clarified. The systematic effects of etching on the six-arm system are evident in *Figure 17*. The dilute solution appeared to etch away a spherulitic layer, approximately 10 μm, in 10 min of etching while the concentrated etchant solution appeared to have the same effect after only 1 min. Thus, a sample etched 10 min in concentrated solution reveals morphology approximately 100 μm beneath the surface. Comparison of spherulitic size, size distribution and shape reveal no significant differences as a function of star-branching. Spherulitic structure suggests three-dimensional growth with an average spherulite diameter on the order of 10 μm for samples crystallized at 200°C (see *Figure 18*). The observed Avrami exponent at 200°C was 3.8. When compared to samples etched 1 min with concentrated solution, no morphological differences are seen in samples etched 10 min as shown by *Figure 17c*, thereby indicating that no noticeable differences are present in bulk *versus* surface morphology on samples cast between PTFE films. The fact that no differences were evident suggests that no major surface nucleation effects are present. The concave surfaces evident on some of the spherulites are the sites of impingement. The fact that these surfaces are non-planar suggests that the spherulites were not nucleated simultaneously, i.e. homogeneous nucleation may have occurred. Three-dimensional growth by homogeneous or self-nucleation would be a phenomenon consistent with an Avrami exponent of four and results obtained earlier by Magill[13]. Lack of surface nucleation may be accounted for by the rapid rate of self-nucleation observed.

The small difference in average spherulite diameter seen in OPM and SALS may be related to differences in the level of impurities or branch-point chemistry, either of which could act as nucleation sites, thereby slightly increasing nucleation density. In any case, the slight variation in nucleation density observed in the three-arm system *versus* the linear and six-arm systems may account for the trend towards slightly higher K values in the three-arm system.

Although no major differences were noted in the size and shape of spherulites, reduced equilibrium melting points in star-branched nylon-6 suggests that some type of structural differences may be present within the crystalline structure of these polymers due

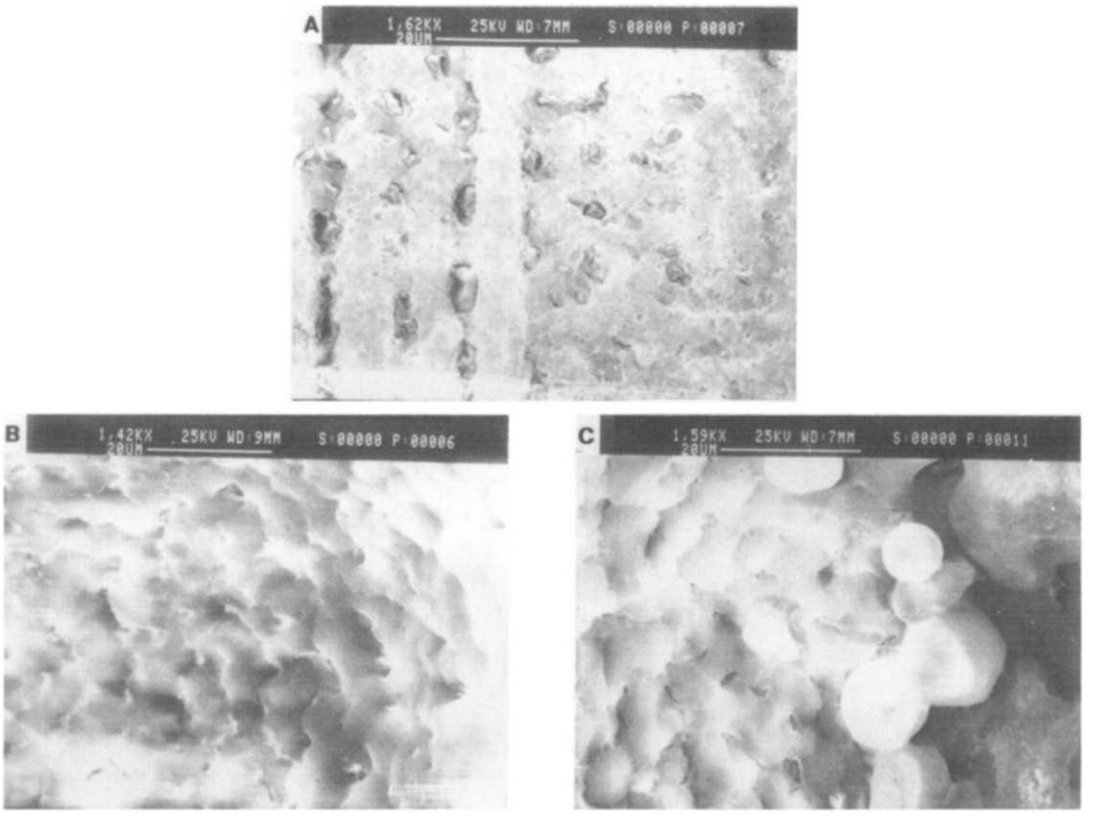

Figure 17 Effects of chemical etching time on six-arm nylon-6 observed by SEM. A – etched 1 min in dilute etchant solution, B – etched 2 min in dilute etchant solution, C – etched 5 min in dilute etchant solution

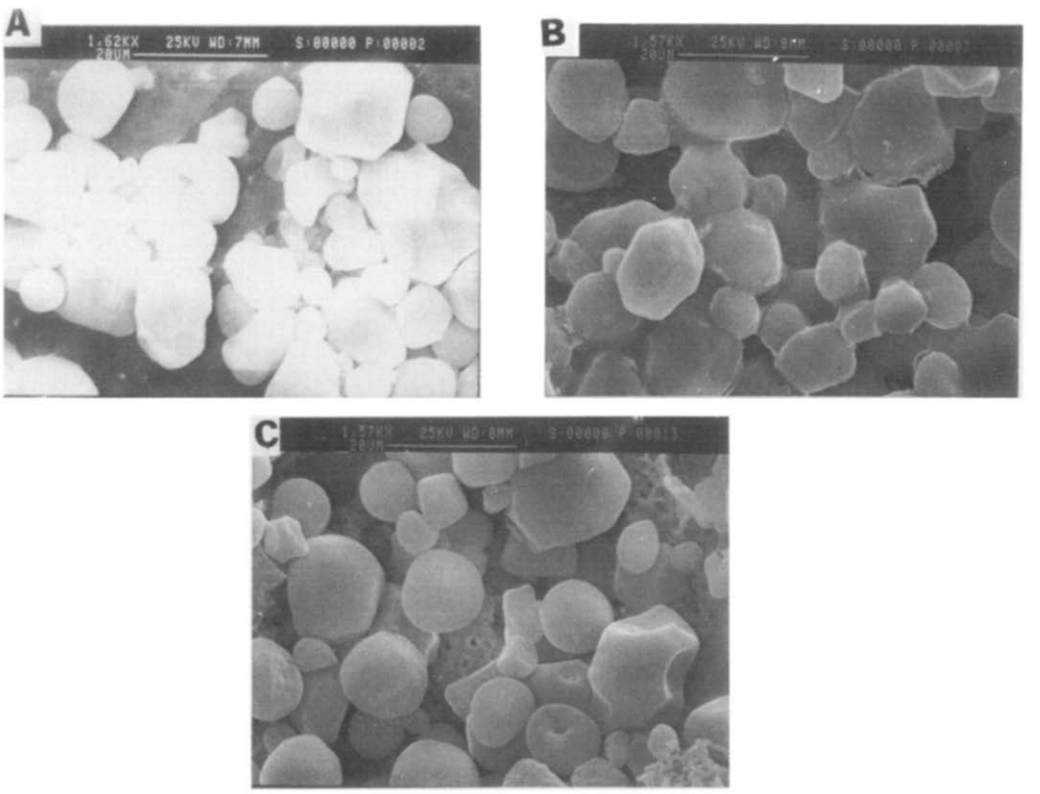

Figure 18 Morphological features of etched linear, three-arm, and six-arm nylon-6 as observed by SEM. A – linear nylon-6, B – three-arm nylon-6, C – six-arm nylon-6

to the presence of branch-points. WAXD failed to reveal any differences in crystal structure or order. SAXS experiments performed on samples isothermally crystallized at 200°C reveal a broadening and decrease in intensity in the scattering peak (*Figure 19*). The linear system displays a strong peak in the smeared SAXS pattern corresponding to an approximate long spacing of 110 Å. Although no significant change in long spacing was observed, the star-branched systems displayed a decreased peak prominence as a function of branch-point functionality. The trend shown in this series of SAXS scans suggests that star-branching disrupts spatial regularity in lamellar structure. The average extended chain length for the linear nylon-6 with $DP=270$ is approximately 2300 Å[46]; in a lamellar crystal 110 Å thick, such a polymer chain could be folded approximately 20 times if both regular folding and adjacent re-entry took place. Since the bulky branch-points are difficult to pack into a crystal lattice, and no differences in lattice structure were observed as a function of branch-point functionality, it is expected that these branch-points exist at the fold surface of the lamellar crystals.

Since the initiator chemistry was different from that of nylon-6 for all samples investigated, it is expected that regular folding may continue only until a branch-point is reached. At this point some disruption of regular folding is expected. The linear system may make up to 10 such regular folds until a chemically different unit is encountered. The three-arm polymer may only make about six regular folds before encountering a branch-point and the six-arm polymer with $DP=270$ may only make about three. Although there is certainly some question as to just how regularly polymer chains are folded in lamellar crystals, it should be noted that each time a fold is made at a branch-point, considerable disruption of regular folding must occur in order to include the rest of the branches. This disruption of regular folding will, most likely, lead to increased fold energies and decreased order at and near the lamellar fold surface. Besides lowering the melting point of a lamellar crystal, branch-points at the fold surface lead to a broader interphase between lamellar crystals and intervening amorphous material. Mandelkern and Popli[47] have shown that small concentrations of branch-points in polyethylene may double the amount of polymer in interfacial regions. Recently Lee *et al.*[48] have shown that increasing the thickness of the interfacial layer between crystalline and amorphous material, while keeping total crystalline percentage constant, leads to substantial attenuation of SAXS peaks. An increase in interfacial material would be consistent with all our experimental findings. Irregularities in the fold surface are consistent with depressed melting points for branched polymer crystals as well as broadened and attenuated SAXS peaks.

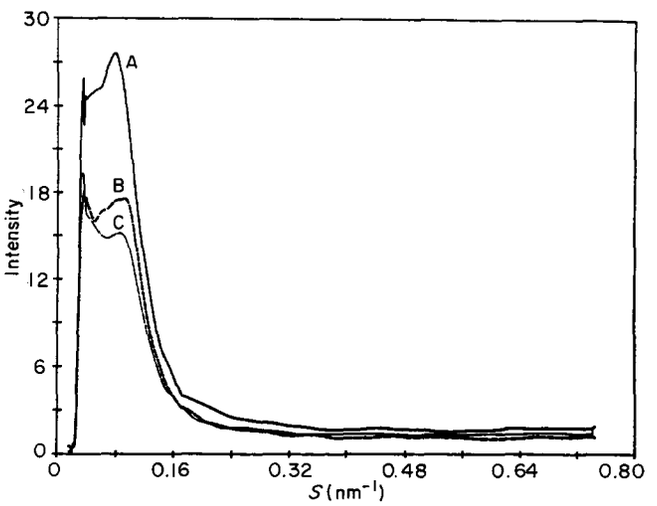

Figure 19 Smoothed, smeared SAXS profiles obtained from nylon-6. A – linear nylon-6, B – three-arm nylon-6, C – six-arm nylon-6

The results of SAXS experiments raised new questions concerning the nature of structural disorder introduced by the inclusion of branch-points within crystalline structure. TEM experiments were performed in order to clarify the details of the lamellar structure in linear *versus* branched nylon-6. No differences were evident in spherulitic superstructure at low magnification (*Figure 20*). Upon higher magnification and even after staining for extended periods of time with RuO_4, no lamellar structure was resolvable in this study. Interestingly, earlier experiments performed by Trent *et al.*[49] using RuO_4 on nylon-11 also failed to reveal lamellar structure.

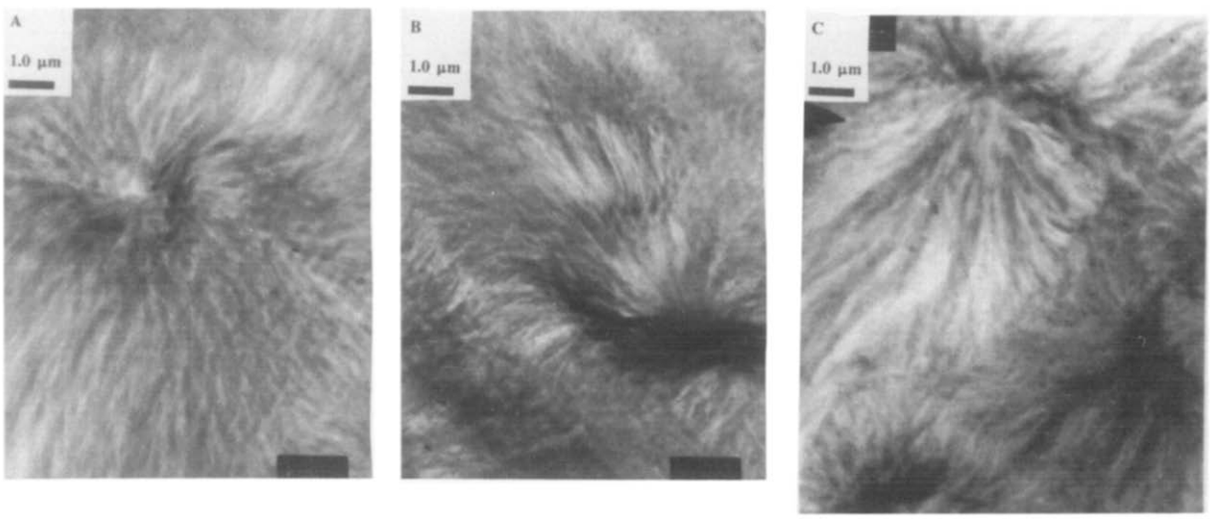

Figure 20 Spherulitic superstructure of nylon-6 stained with RuO_4 as observed by TEM. A – linear nylon-6: crystallized at 200°C, B – three-arm nylon-6: crystallized at 200°C, C – six-arm nylon-6: crystallized at 200°C

CONCLUSIONS

The effect of star-branching functionality on the morphology, crystallization kinetics, equilibrium melting point and heat of fusion of nylon-6 was studied by OPM, SALS, SEM, WAXS, SAXS, TEM and d.s.c. The crystallization kinetics of all three systems could be described by an Avrami equation with exponents, on average, between 2.8 and 4.5. As first noted by Magill, a transition from heterogeneous nucleation to homogeneous nucleation of spherulites at 197°C is consistent with the observed change in Avrami exponent of linear and star-branched nylon-6. No significant differences in either Avrami exponent or rate constant as a function of temperature were observed as a function of increasing branch-point functionality. However, crystallization half-times were reduced by one-half in the branched systems for equivalent values of *supercooling*. Crystallization half-times may be affected by reduced reptation times in these star-branched systems. Although melting points appeared to be systematically lowered with increasing branch-point functionality, no significant differences were observed in absolute crystalline percentages. SAXS measurements suggest that irregularities at or near the surface of lamellar crystals containing branched macromolecules may be responsible for the observed depression of melting points. If the ratio (M_w/M_e) is kept low, star-branching may be a feasible way in which the melt viscosity and crystallization half-times of nylon-6 can be substantially reduced. Controlled star-branching of polymers may lead to improvements in both processability and bulk crystallization rates.

ACKNOWLEDGEMENTS

The authors appreciate the support of this research by the National Science Foundation Science and Technology Center for High Performance Polymeric Adhesives and Composites at Virginia Polytechnic under contract number DMR8809714, as well as the Dow Chemical Company and Phillips Petroleum Company. We would also like to recognize Will Hartt and Professor Don Baird for their assistance in rheological measurements and Professor Saverio Russo for his assistance in specimen characterization.

REFERENCES

1 Tomalia, D. A. *et al. Polym. J.* 1985, **17**, 117
2 Devlin, B. P. and Tirrell, D. A. *Macromolecules* 1986, **19**, 2466
3 Tomalia, D. A., Hall, M. and Hedstrand, D. M. *J. Am. Chem. Soc.* 1987, **109**, 1601
4 Tomalia, D. A., Berry, V., Hall, M. and Hedstrand, D. M. *Macromolecules* 1987, **20**, 1167
5 Warakomski, J. M. *Polym. Prepr.* 1989, **30**, 117
6 Xenopoulos, A. and Wunderlich, B. *J. Polym. Sci.* (B) 1990, **28**, 2271
7 Khanna, Y. P. and Reimschuessel, A. C. *J. Appl. Polym. Sci.* 1988, **35**, 2259
8 Khanna, Y. P., Reimschuessel, A. C., Banerjie, A. and Altman, C. *Polym. Eng. Sci.* 1988, **28**, 1600
9 Khanna, Y. P., Kumar, R. and Reimschuessel, A. C. *Polym. Eng. Sci.* 1988, **28**, 1607
10 Khanna, Y. P., Kumar, R. and Reimschuessel, A. C. *Polym. Eng. Sci.* 1988, **28**, 1612
11 Patel, R. P. and Spruiell, J. E. *Polym. Eng. Sci.* 1991, **31**, 730
12 Frunze, T. M. *et al. Polym. Sci. USSR* 1972, **A14**, 962
13 Magill, J. H. *Polymer* 1962, **3**, 655
14 Mathias, L. J. and Sikes, A. M. *Polym. Mater. Sci. Eng.* **56**, 87
15 Mathias, L. J. and Sikes, A. M. *ACS Symp. Ser.* 1988, **367**, 66
16 Hser, J.-C. and Carr, S. H. *Polym. Eng. Sci.* 1979, **19**, 436
17 Warakomski, J. M. *Chem. Mater.* in press
18 Russo, S. private communication
19 Russo, S., Biagani, E., Gattiglia, E. and Pedemonte, E. *Macromol. Chem.* 1983, **184**, 1213
20 Russo, S. *et al. Polymer* 1987, **28**, 114
21 Zimm, B. and Stockmayer, W. H. *J. Chem. Phys.* 1949, **17**, 1301
22 Sawyer, L. C. and Grubbs, D. T. 'Polymer Microscopy', Chapman and Hall, New York, 1987
23 Olley, R., Basset, D. and Blundell, D. *Polymer* 1986, **27**, 344
24 Wilkes, G. L. 'Encyclopedia of Polymer Science and Engineering', 2nd edn, Vol. 14, 1988, p. 542
25 Hermans, P. H. and Weidinger, A. *Text. Res. J.* 1961, **31**, 558
26 Vonk, C. G. *J. Appl. Cryst.* 1973, **6**, 148
27 Murthy, N. S., Curran, S. A., Aharoni, S. M. and Minor, H. *Macromolecules* 1991, **24**, 3215
28 Janzen, J. private communication
29 Ruland, W. *Polymer* 1964, **5**, 89
30 Bandrup and Immergut (Eds) 'Polymer Handbook', 2nd edn, 1975, p. III-25
31 Avrami, M. *J. Chem. Phys.* 1939, **7**, 1103; *J. Chem. Phys.* 1940, **8**, 212; *J. Chem. Phys.* 1941, **9**, 177
32 Wunderlich, B. 'Macromolecular Physics, Crystal Nucleation, Growth, Annealing', Vol. 2, Academic Press, New York, 1976
33 Hoffman, J. D. and Weeks, J. J. *J. Res. Natl. Bur. Stand.* (*A*) 1962, **66**, 13
34 Hoffman, J. D., Davis, G. T. and Lauritzen Jr, J. I. in 'Treatise on Solid State Chemistry' (Ed. N. B. Hannay), Plenum Press, New York, 1976, Vol. 3, Ch. 7
35 Roland, M. C. and Buckley, G. S. *Rubber Chem. Technol.* 1990, **64**, 74
36 de Gennes, P. G. *J. Phys.* (Paris) 1975, **36**, 1199
37 Ngai, K. L., Rajagopal, A. K. and Lodge, T. P. *J. Polym. Sci. B* 1990, **28**, 1367
38 Lodge, T. P., Markland, P. and Wheeler, L. M. *Macromolecules* 1989, **22**, 3409
39 Viovy, J. L., Rubinstein, M. and Colby, R. H. *Macromolecules* 1990, **24**, 3587
40 Roovers, J. *Macromolecules* 1991, **24**, 5895
41 Ngai, K. L. and Plazek, D. J. *J. Polym. Sci., Polym. Phys.* 1985, **23**, 2159
42 Boyer and Miller *Rubber Chem. Technol.* 1978, **51**, 718
43 Doi, M. and Edwards, S. F. 'The Theory of Polymer Dynamics', Clarendon, Oxford, 1986
44 Lodge, T. P., Rotstein, N. A. and Prager, S. *Adv. Chem. Phys.* 1990, **79**, 1
45 Zimm, B. and Stockmayer, W. H. *J. Chem. Phys.* 1945, **17**, 1301
46 Calleja and Keller *J. Polym. Sci.* 1964, **A2**, 2151
47 Popli, R. and Mandelkern, L. *J. Polym. Sci., Part B: Polym. Phys.* 1987, **25**, 441
48 Lee, Y. D., Phillips, P. J. and Lin, J. S. *J. Polym. Sci. B Polym. Phys.* 1991, **29**, 1235
49 Trent, J. S., Scheinbeim, J. I. and Couchman, P. R. *Macromolecules* 1983, **16**, 589